Zinc plays a key role in human and bacterial GTP cyclohydrolase I

Günter Auerbach*†, Anja Herrmann‡§, Andreas Bracher‡¶, Gerd Bader*, Markus Gütlich‡, Markus Fischer‡, Martin Neukamm‖, Marta Garrido-Franco*, John Richardson*, Herbert Nar*,, Robert Huber*, and Adelbert Bacher‡††**

*Abteilung Strukturforschung, Max-Planck-Institut für Biochemie, Am Klopferspitz 18a, D-82152 Martinsried, Germany; and ‡Lehrstuhl für Organische Chemie und Biochemie, and ‖Lehrstuhl für Technische Chemie, Technische Universität München, Lichtenbergstr. 4, D-85747 Garching, Germany

Contributed by Robert Huber, September 28, 2000

The crystal structure of recombinant human GTP cyclohydrolase I was solved by Patterson search methods by using the coordinates of the *Escherichia coli* enzyme as a model. The human as well as bacterial enzyme were shown to contain an essential zinc ion coordinated to a His side chain and two thiol groups in each active site of the homodecameric enzymes that had escaped detection during earlier studies of the *E. coli* enzyme. The zinc ion is proposed to generate a hydroxyl nucleophile for attack of imidazole ring carbon atom eight of the substrate, GTP. It may also be involved in the hydrolytic release of formate from the intermediate, 2-amino-5-formylamino-6-ribosylamino-4(3*H*)-pyrimidinone 5′-triphosphate, and in the consecutive Amadori rearrangement of the ribosyl moiety.

GTP cyclohydrolase I (GTP-CH-I; E.C. 3.5.4.16) catalyzes the conversion of GTP to dihydroneopterin triphosphate (H_2NTP, 6-D-*threo*-1′,2′,3′-hydroxypropyl-7,8-dihydroneopterin 3′-triphosphate). In plants and certain microorganisms, the enzyme product serves as the first committed intermediate in the biosynthesis of tetrahydrofolate (1). In animals, dihydroneopterin triphosphate is converted to tetrahydrobiopterin (BH_4, [6*R*]-[L-erythro-1′,2′-dihydroxypropyl]-2-amino-4-hydroxy-5,6,7,8-tetrahydropteridine) by the sequential action of 6-pyruvoyl tetrahydropterin synthase (PPH_4S, PTPS; E.C. 4.6.1.10) and sepiapterin reductase (E.C. 1.1.1.153) (2).

Tetrahydrobiopterin functions as an essential cofactor for nitric oxide synthases, glycerol ether monooxygenases, and pterin-requiring monooxygenases (phenylalanine hydroxylase in liver, tyrosine hydroxylase in catecholamine-containing cells, and tryptophan hydroxylase in serotonin-containing cells) (2). Tetrahydrobiopterin availability appears to limit the activity of these enzymes and may therefore influence the rate of production of several key cell-signaling molecules (nitric oxide, dopamine, norepinephrine, epinephrine, and serotonin).

Tetrahydrobiopterin levels in mammalian cells are mainly determined by GTP-CH-I activity. Mutations in the GTP-CH-I gene are responsible for severe diseases including dopa-responsive dystonia (3) and certain cases of atypical phenylketonuria (4). Mammalian GTP-CH-I is inhibited by tetrahydrobiopterin and stimulated by phenylalanine through complex formation with the GTP-CH-I feedback regulatory protein (5, 6).

The structures of *Escherichia coli* GTP cyclohydrolase I (eGTP-CH-I) (7), rat liver 6-pyruvoyl tetrahydropterin synthase (8, 9), and mouse sepiapterin reductase (10) have been determined by x-ray crystallography; eGTP-CH-I is a toroid-shaped, D5-symmetric homodecamer (11). The 10 equivalent active sites are located at the periphery of the toroid, and each catalytic site is located at the interface of three adjacent subunits.

Reaction mechanisms for GTP-CH-I have been proposed on the basis of biochemical and crystallographic studies (12, 13), but the details of the complex reaction sequence remained incompletely understood. A much clearer view of this intriguing reaction sequence becomes possible by the discovery of an essential zinc ion at the active site of the enzyme which is described in this paper.

Materials and Methods

Microorganisms. Bacterial strains and plasmids used in this study are summarized in Table 1.

Construction of an Expression Plasmid for Human GTP-CH-I (hGTP-CH-I). A PCR using the plasmid pMAL-GTP-CH-I (Table 1) as template and the oligonucleotides hGTP-CH-42 and hGTP-CH-*Bam*HI (2) as primers afforded an amplificate of 655 bp that was purified and used as template in a second PCR round with the oligonucleotides Uni-*Eco*RI and hGTP-CH-42 as primers (Table 2). The amplificate was purified, digested with the restriction endonucleases *Bam*HI and *Eco*RI, and ligated into the plasmid p602-CAT (14) which had been treated with the same restriction endonucleases. The resulting plasmid p602-hGTP-CH-42 was electrotransformed into the *E. coli* strain M15[pGB3] (15) harboring the pGB3 plasmid which directs the overexpression of *lac* repressor protein. The sequence of plasmid p602-hGTP-CH-42 has been deposited in the European Molecular Biology Laboratory database (accession no. AF288421).

Enzyme Assay. GTP-CH-I activity was monitored as described (2, 16).

Purification of Δ42-hGTP-CH-I. A culture of recombinant *E. coli* M15[pGB3](p602-hGTP-CH-42 was grown in terrific broth (17) containing ampicillin (150 mg/liter)/kanamycin (20 mg/liter)/1 mM isopropyl-β-D-thiogalactopyranoside. The culture was incubated for 24–36 h at 37°C and was harvested by centrifugation (5,000 rpm for 10 min at 4°C). The pellet was washed with 0.9% NaCl and resuspended in buffer A [50 mM Tris·HCl (pH 8.0)/2 mM 1,4-DTT/0.02% NaN_3). The suspension was ultrasonically treated and centrifuged (15,000 rpm for 20 min at 4°C). PMSF was added to a final concentration of 1 mM. The subsequent chromatographic steps were carried out at 4°C.

Abbreviations: GTP-CH-I, GTP cyclohydrolase I; eGTP-CH-I, *Escherichia coli* GTP cyclohydrolase I; hGTP-CH-I, human GTP cyclohydrolase I.

Data deposition: The atomic coordinates and structural factors have been deposited in the Protein Data Bank, www.rcsb.org (PDB ID codes 1FB1 and 1FBX).

†Present address: Antisense Pharma GmbH, Josef-Engert-Str. 9, D-93053 Regensburg, Germany.

§Present address: Microcoat GmbH, Am Neuland 1, D-82347 Bernried, Germany.

¶Present address: EMBL Grenoble, 6 rue Jules Horowitz, F-38000 Grenoble, France.

**Present address: Boehringer Ingelheim Pharma Deutschland, Structural Research, Birkendorferstrasse 65, D-88400 Biberach, Germany.

††To whom reprint requests should be addressed. E-mail: adelbert.bacher@ch.tum.de.

The publication costs of this article were defrayed in part by page charge payment. This article must therefore be hereby marked "*advertisement*" in accordance with 18 U.S.C. §1734 solely to indicate this fact.

Article published online before print: *Proc. Natl. Acad. Sci. USA*, 10.1073/pnas.240463497. Article and publication date are at www.pnas.org/cgi/doi/10.1073/pnas.240463497

Table 1. Bacterial strains and plasmids used in this study

Strains and plasmids	Name
Bacterial strains	*E. coli* XL1Blue
	E. coli M15[pGB3])
Plasmids	p602/-CAT
	pMAL-GTP-CH-I
	p602-hGTP-CH-42 (accession no. AF288421)

The supernatant was loaded on a Sepharose Q-FastFlow column (2.5 × 12 cm, Amersham Pharmacia) equilibrated with buffer A. The column was washed with 120 ml of buffer A and developed with a linear gradient of 0 to 100% buffer B containing 50 mM Tris·HCl (pH 8.0)/200 mM KCl/2 mM 1,4-DTT/0.02% NaN_3 (total volume, 650 ml). Fractions were combined, and solid ammonium sulfate was added to a final concentration of 1 M. During the addition, the pH value was adjusted to 7.5 by the addition of 10 mM NaOH. After 30 min at 4°C, the suspension was centrifuged (15,000 rpm for 20 min at 4°C), and the supernatant was applied to a Butyl Sepharose column (2.5 × 3 cm, Amersham Pharmacia) which had been equilibrated with buffer C [50 mM potassium phosphate (pH 7.5)/1 M ammonium sulfate/2 mM 1,4-DTT/0.02% NaN_3). The column was washed with 100 ml of buffer C and was then developed with a linear gradient of 1 to 0 M ammonium sulfate/50 mM potassium phosphate (pH 7.5)/2 mM 1,4-DTT/0.02% NaN_3 (total volume, 100 ml). Fractions were combined and concentrated. The solution was applied to a Superdex 200 Prepgrade column (6 × 16 cm, Amersham Pharmacia) equilibrated with buffer D [100 mM potassium phosphate (pH 7.5)/2 mM 1,4-DTT/0.02% NaN_3].

Purification of eGTP-CH-I. *E. coli* strain M15 REPECHI was grown as described (16). The recombinant protein was purified as described (16); EDTA was omitted from all buffers.

Estimation of Protein Concentration. The concentration of Δ42-hGTP-CH-I was estimated photometrically by using an absorbance coefficient of $\varepsilon_{280} = 15{,}900\ M^{-1}\cdot cm^{-1}$.

Atomic Absorption Spectroscopy. Purified protein (1.3–1.6 mg/ml) was dialyzed against 5 mM Tris·HCl (pH 8.0). The solution was analyzed in a graphite furnace atomic absorption spectrograph Unicam 939 from Perkin–Elmer. The dialysis buffer was used as reference, and 0.1 M zinc sulfate (Fluka) was used as standard.

Crystallization of Δ42-hGTP-CH-I. Protein solution [4.6 mg/ml 100 mM potassium phosphate (pH 7.5)/2 mM 1,4-DTT/0.02% NaN_3) was mixed with one aliquot of 1.0 M ammonium sulfate (pH 7.5)/3.2% isopropanol/2 mM DTT. Hanging drops were equilibrated with the precipitant solution at 20°C.

Crystallization of Recombinant eGTP-CH-I. Three aliquots of eGTP-CH-I (6 mg/ml) in 10 mM potassium phosphate (pH 7.0)/0.02% NaN_3 were mixed with an aliquot of a solution containing 6% PEG 6000/150 mM KCl/100 mM 4-morpholinepropanesulfonic acid (pH 7.0). Crystallization drops were equilibrated with the precipitant solution.

Data Collection. A data set of the recombinant human enzyme was collected at 277 K to a resolution of 3.1 Å by using nine crystals and a MAR-Research (Hamburg, Germany) imaging plate system at the DESY BW6 synchrotron radiation beam line Hamburg (λ = 1.07 Å; 1.0° frames) (Table 3). A native data set of eGTP-CH-I crystals to a resolution of 2.8 Å was obtained with a rotating Cu-K_α radiation source and a MAR-Research imaging plate (Table 4).

Data Processing. Images were indexed and integrated with the MOSFLM package (18) and further processed by using the CCP4 suite of programs (19). A total of 25,288 unique reflections above 2 σ (276,838 total measurements) was collected for Δ42-hGTP-CH-I representing 84.5% of the possible data to a resolution of 3.1 Å. The data are 41.9% complete in the outermost resolution shell. In the case of eGTP-CH-I, 107,321 unique reflections above 2 σ (572,885 total measurements) were collected. The data are 90.2% complete (44.3% in the outer shell).

Structure Determination. The crystal structure of Δ42-hGTP-CH-I was solved by Patterson search techniques (20, 21) by using the coordinates of the pentamer of wild-type eGTP-CH-I (7) as a search model. The program AMORE (22) was used in the resolution range from 15.0 to 4.0 Å with an integration vector of 20 Å. The highest solution found had 5-fold symmetry, a correlation coefficient of 0.435, and a *R* factor of 47.8%. The next highest peak had a correlation coefficient of 0.355 and a *R* factor of 50.7%. The structure of the zinc-containing *E. coli* enzyme could be analyzed by using phases of the isomorphous zinc-depleted enzyme.

Model Building and Refinement. The initial electron density was modified applying noncrystallographic symmetry averaging with the program MAIN (23). Model building was done with O (24) and refinement with X-PLOR (25) resp. CNS (26). Noncrystallographic symmetry restraints were applied during refinement of the five (15) monomers per asymmetric unit in the crystals of the human (bacterial) enzyme. They were relaxed at the final stages, resulting in a NCS tissue solubilizer (Amersham International) rms deviation of 0.78 Å. The human (bacterial) enzyme model was refined to *R* factors of 21.6% (20.2%) and R_{free} of 29.3% (25.4%). The rms deviations from ideal stereochemistry (27) of the human (bacterial) enzyme model are 0.011 Å (0.011 Å) for bond lengths and 1.61° (1.47°) for bond angles. The final model of the human (bacterial) enzyme contains 7,735 (25,965) nonhydrogen atoms and five isopropanol molecules (15 water molecules). One zinc ion per monomer was found in both enzymes. Ribbon representations were drawn with the programs MOLSCRIPT (28) and RENDER (29). Coordinates have been deposited in the RCSB Protein Data Bank with identity codes 1FB1 (Δ42-hGTP-CH-I) and 1FBX (eGTP-CH-I).

Results and Discussion

Expression of Δ42-hGTP-CH-I in a Recombinant *E. coli* Strain. A recombinant *E. coli* strain with a plasmid directing the synthesis of full-length hGTP-CH-I under the control of a *lac* operator and *lac* promoter produced a recombinant peptide with an apparent relative mass of 27.9 kDa. All attempts to purify this protein

Table 2. Oligonucleotides used in this study

Designation	Sequence
hGTP-CH-42	5′-GAG GAG AAA TTA ACT ATG CCG GAA GCG AAG AGC GCG CAG CCC-3′
hGTP-CH-*Bam*HI	5′-G GTC GAC GGA TCC TCA GCT CCT AAT GAG AGT CAG G-3′
Uni-*Eco*RI	5′-CAA TTT GAA TTC ATT AAA GAG GAG AAA TTA ACT ATG-3′

Table 3. Data collection and refinement statistics of the crystal structure of hGTP-CH-I in complex with zinc

Data collection	
Resolution range, Å	20–3.1
Observed reflections	276,838
Unique reflections	25,288
R_{merge}	0.165
Completeness, % (overall/outer shell)	84.5/41.9
Refinement	
Resolution range, Å	20.0–3.1
R_{cryst}	0.216
R_{free}	0.293
No. of protein atoms	7,735
rmsd bond lengths, Å	0.011
rmsd angles, °	1.61
rmsd between monomers, Å (C_α atoms)	0.42
Mean *B* factor, Å^2	88.68

Table 4. Data collection and refinement statistics of the crystal structure of eGTP-CH-I in complex with zinc

Data collection	
Resolution range, Å	20–2.8
Observed reflections	572,885
Unique reflections	107,321
R_{merge}	0.12
Completeness, % (overall/outer shell)	90.2/44.3
Refinement	
Resolution range, Å	15–2.8
R_{cryst}	0.202
R_{free}	0.254
No. of protein atoms	25,965
rmsd bond lengths, Å	0.011
rmsd angles, °	1.47
rmsd between monomers, Å	0.19
Mean *B* factor, Å^2	44.0

yielded mixtures of partially proteolyzed polypeptides as shown by SDS/PAGE. N-terminal sequencing showed that different subunits had been proteolyzed at any one of eight Arg residues in the N-terminal stretch of 41 residues, affording a variety of cleavage products.

An attempt was made to increase the stability of the recombinant protein by the successive substitution of these Arg residues by Gln residues. A stable protein species was ultimately obtained after exchange of all nine respective Arg residues by Gln. The modified protein could be purified to apparent homogeneity and had uncompromised enzyme activity but failed to crystallize, possibly as a consequence of intermolecular steric hindrance caused by the N-terminal peptide segment.

A gene cassette specifying a peptide subunit with a deletion of amino acid residues 2–41 was then constructed. This gene construct directed the synthesis of a protein (subsequently designated Δ42-hGTP-CH-I) with an apparent mass of 23 kDa in a recombinant *E. coli* strain. The recombinant protein could

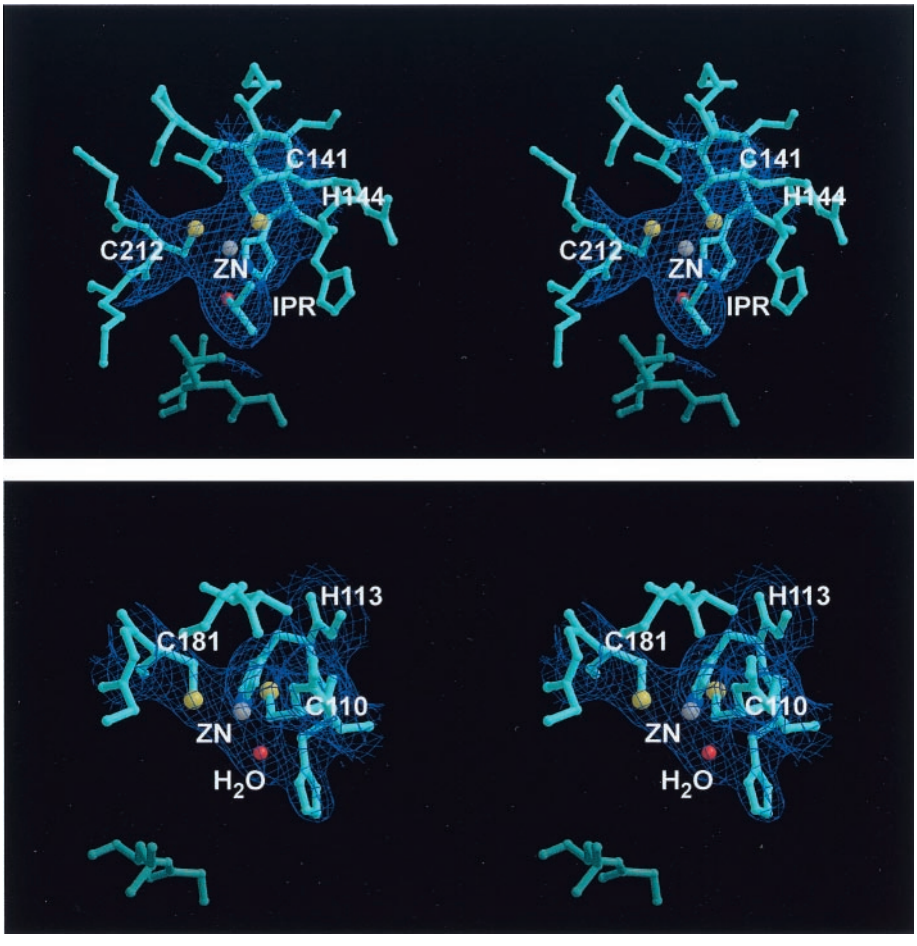

Fig. 1. Stereo view of the active site of (*a*) hGTP-CH-I and (*b*) eGTP-CH-I harboring zinc. The averaged $2F_o - F_c$ electron density maps are shown in blue.

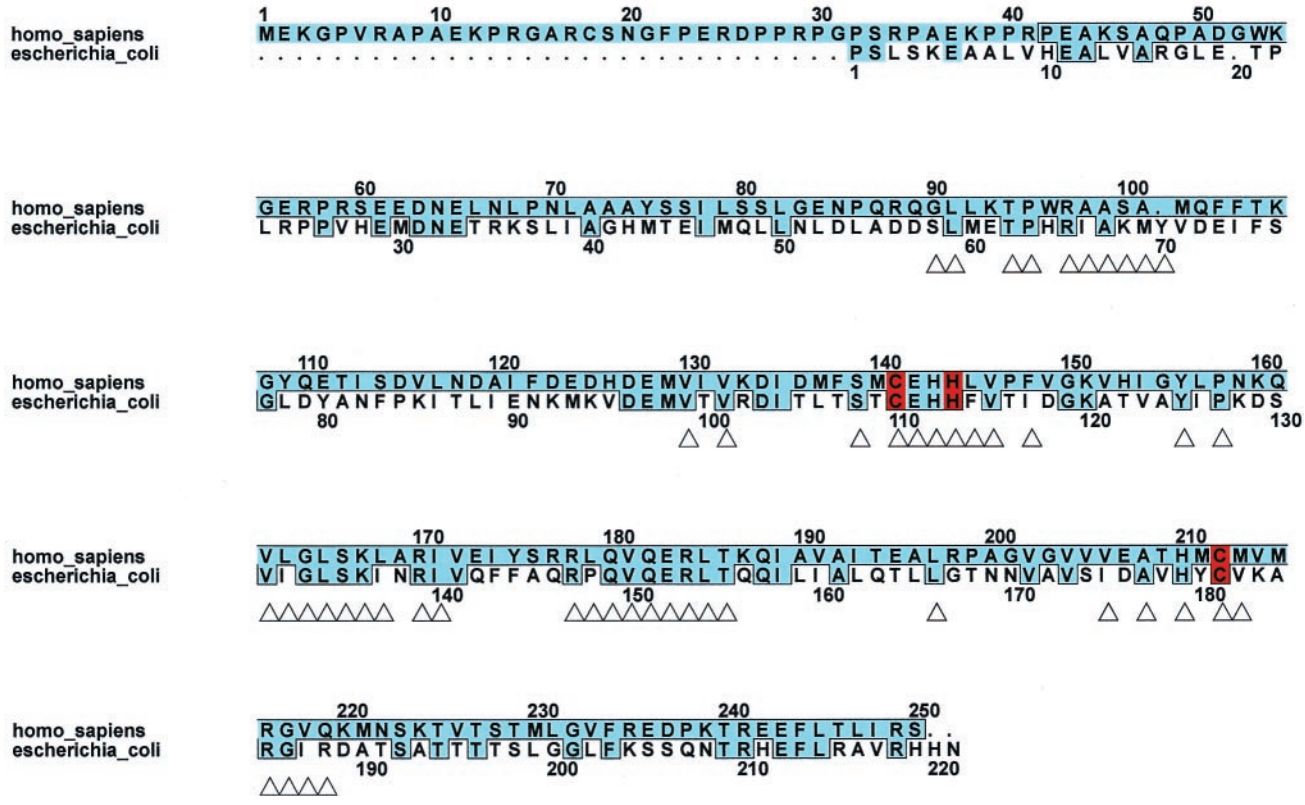

Fig. 2. Sequence alignment of hGTP-CH-I (numbering above) and eGTP-CH-I (numbering below). Residues, which are identical with hGTP-CH-I, are highlighted in blue, and if part of the hGTP-CH-I model, additionally framed. (△) Residues with a distance below 10 Å around the active site. Amino acid residues involved in zinc binding are marked in red.

be purified to homogeneity without apparent degradation. The catalytic activity of the truncated protein was closely similar to that of the full-length recombinant protein. Moreover, the truncated protein was subject to inhibition by GTP-CH-I feedback regulatory protein in close similarity with the properties of the full-length protein.

Crystallization and Structure Determination of Δ42-hGTP-CH-I. Crystals of Δ42-hGTP-CH-I grew to a size of 700 μm within a few days. The crystals belong to the hexagonal space group $P6_522$ with five monomers in the asymmetric unit and lattice constants $a = b = 115.1$ Å, and $c = 387.3$ Å. The solvent content of the crystals is 60%, corresponding to a Matthews parameter of $V_m = 3.04$ Å^3/Da.

By using nine crystals, a complete data set could be collected to a resolution of 3.1 Å. The structure was solved by Patterson search techniques by using the pentamer model of the *E. coli* enzyme. The refined model includes amino acid residues 17–209 of the 209-residue sequence of each of the five monomers in the asymmetric unit of Δ42-hGTP-CH-I.

Zinc Bound to the Active Site of Human GTP-CH-I. The crystal structure revealed a metal ion bound to His-143 and the sulfhydryl groups of Cys-141 and Cys-212 at the active site that was identified as zinc by atomic absorption spectrometry. An isopropanol molecule from the crystallization buffer was bound to the zinc ion (Fig. 1).

Crystallographic Analysis of eGTP-CH-I Purified in the Absence of Chelating Agents. In light of the detection of a zinc ion at the active site of the human protein, we reinvestigated the *E. coli* protein particularly in relation to the metal content. The purification of the recombinant *E. coli* protein used in earlier crystallographic studies had invariably involved the use of buffers containing EDTA. The resulting protein had shown specific activities around 20 nmol/mg/min (30). Recombinant *E. coli* protein purified without a chelating agent had a specific activity of 96 nmol/mg per min (16). Crystals of this enzyme batch were obtained as reported earlier and grew within 2 weeks to sizes of 0.5 mm. X-ray diffraction data collected to a resolution of 2.8 Å indicated unit-cell dimensions of $a = 227.7$ Å, $b = 314.2$ Å, and $c = 132.6$ Å and space group $C222_1$ similar to the previous crystals (12). The active sites of the *E. coli* and human enzyme are shown in Fig. 1. Electron density between the sulfhydryl groups of the Cys-110 (-141) and Cys-181 (-212) and His-113 (-143) suggested strongly a bound metal ion. Chemical analysis indicated 0.9 ± 0.1 zinc ions per protein subunit.

In retrospect, it appears obvious that the disulfide bridge observed earlier in the *E. coli* protein (7) had been an oxidation artifact caused by metal depletion of the protein. Moreover, the low specific activities of the protein used in the earlier crystallographic studies had been caused by the partial zinc depletion. It should also be mentioned that replacement of any amino acid residue directly involved in the chelation of the essential zinc ion results in protein devoid of zinc and loss of catalytic activity (12).

Comparison of hGTP-CH-I with the Bacterial Enzyme. The sequence identity of hGTP-CH-I with the bacterial enzyme is 37% (Fig. 2). Similar to the bacterial enzyme, the monomer of hGTP-CH-I folds into an $\alpha\beta$ structure and oligomerizes to a doughnut-shaped homodecamer. The amino acid residues involved in substrate binding and catalysis are strictly conserved. Superposition of both enzyme structures reveals a rms deviation of 1.25

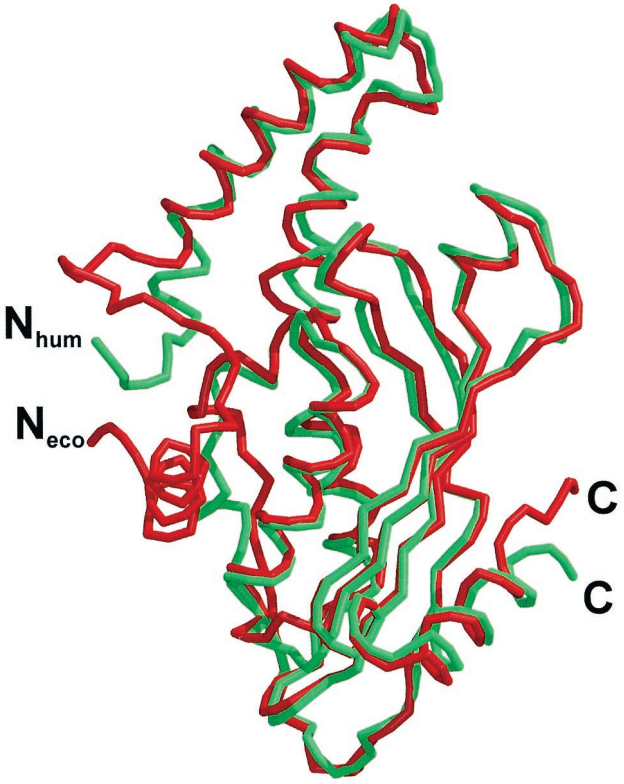

Fig. 3. Superposition of the monomers of hGTP-CH-I (green) and eGTP-CH-I (red). The termini of both human (hum) and *E. coli* (eco) enzyme are labeled.

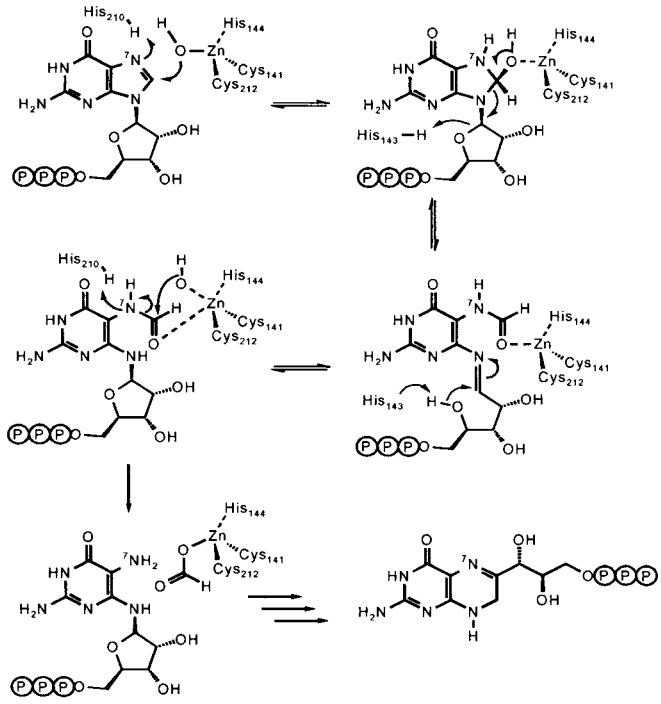

Fig. 4. Hypothetical reaction mechanism for GTP-CH-I.

Å over all five monomers in the asymmetric unit of the hexagonal human crystals (Fig. 3).

Site-directed mutagenesis of the *E. coli* enzyme had shown earlier that the catalytic activity of GTP-CH-I is highly sensitive to the replacement of amino acid residues in the active site cavity (12). Besides the residues Cys-110 (-141), Cys-181 (-212), and His-113 (-144) involved in the complexation of zinc, the amino acids His-112 (-143) and His-179 (-210) are indispensable for the formation of the product dihydroneopterin triphosphate. Residues in brackets are the human equivalents.

Superposition of human and bacterial GTP-CH-I indicates that the N-terminal region missing in the human structure model is probably located at the equator of the toroidal decamer and not involved in substrate binding or catalysis.

Mechanistic Role of Zinc. The zinc ion polarizes its water ligand by enhancing its acidity, thus generating a hydroxyl nucleophile in close proximity of the imidazole ring of the bound substrate whose position had been determined previously (12) (Fig. 4). The zinc-bound hydroxyl ligand could attack carbon atom 8 of GTP, whereas His-179 (-210) could act as a proton donor for nitrogen atom 7 of the substrate. However, because mutants of eGTP-CH-I lacking this His residue catalyze the ring opening step (13), protonation at nitrogen atom 7 by a zinc-activated water molecule appears also possible. As proposed earlier (12), protonation of the furanose ring oxygen atom by His-112 (-143) could assist the opening of the imidazole ring via transient generation of a Schiff base from the *N*-glycoside. The formation of the *N*-glycoside product, 2-amino-5-formylamino-6-ribofuranosylamino-4(3*H*)-pyrimidinone-5′-triphosphate, has been confirmed by studies with His-179 (-210) mutants of eGTP-CH-I (13).

The subsequent cleavage of the formamide bond resembles the reaction catalyzed by zinc proteases. Zinc could simultaneously polarize the formamide carbonyl bond and activate a water molecule for nucleophilic attack. However, in contrast to the initial attack on the imidazole ring, acid catalysis by His-179 (-210) is essential for this step (13).

Whether zinc is involved in the following Amadori rearrangement remains unknown. In any case, a strong base may be required for the necessary abstraction of the proton at carbon atom 2′ of the substrate (16), and a hydroxyl ion generated by zinc (acting again as a Lewis acid) could hypothetically serve that purpose.

We thank Gabi Bergauer and Angelika Werner for expert help with the preparation of the manuscript, and Dr. Hans D. Bartunik and his collaborators for assistance during crystallographic data collection at the BW6 beam line at DESY (Hamburg, Germany). This work was supported by the Deutsche Forschungsgemeinschaft, European Community Grants ERB CHRX CT93–0243 and ERB FMRX-CT98–0204, the Fonds der Chemischen Industrie, and the Hans-Fischer-Gesellschaft.

1. Brown, G. M. & Williamson, J. M. (1987) *Escherichia coli and Salmonella typhimurium,* ed. Neidhardt, F. C. (Am. Soc. Microbiol., Washington, DC), Vol. 1, pp. 521–538.
2. Kaufman, S. (1993) *Annu. Rev. Nutr.* **13,** 261–286.
3. Ozelius, L. J. & Breakefield, X. O. (1994) *Nat. Genet.* **8,** 207–209.
4. Thöny, B., Auerbach, G. & Blau, N. (2000) *Biochem. J.* **347,** 1–16.
5. Yoneyama, T. & Hatakeyama, K. (1998) *J. Biol. Chem.* **273,** 20102–20108.
6. Kapatos, G., Hirayama, K., Shimoji, M. & Milstien, S. (1999) *J. Neurochem.* **72,** 669–675.
7. Nar, H., Huber, R., Meining, W., Schmid, C., Weinkauf, S. & Bacher, A. (1995) *Structure (London)* **3,** 459–466.
8. Nar, H., Huber, R., Heizmann, C. W., Thöny, B. & Bürgisser, D. (1994) *EMBO J.* **13,** 1255–1262.
9. Ploom, T., Thöny, B., Yim, J., Lee, S., Nar, H., Leimbacher, W., Richardson, J., Huber, R. & Auerbach, G. (1999) *J. Mol. Biol.* **286,** 851–860.
10. Auerbach, G., Herrmann, A., Gütlich, M., Fischer, M., Jacob, U., Bacher, A. & Huber, R. (1997) *EMBO J.* **16,** 7219–7230.
11. Auerbach, G. & Nar, H. (1997) *J. Biol. Chem.* **378,** 185–192.

12. Nar, H., Huber, R., Auerbach, G., Fischer, M., Hösl, C., Ritz, H., Bracher, A., Meining, W., Eberhardt, S. & Bacher, A., (1995) *Proc. Natl. Acad. Sci. USA* **92,** 12120–12125.
13. Bracher, A., Fischer, M., Eisenreich, W., Ritz, H., Schramek, N., Boyle, P., Gentili, P., Huber, R., Nar, H., Auerbach, G., *et al.* (1999) *J. Biol. Chem.* **274,** 16727–16735.
14. Mörtl, S., Fischer, M., Richter, G., Tack, J., Weinkauf, S. & Bacher, A. (1996) *J. Biol. Chem.* **271,** 33201–33207.
15. Stüber, D., Matile, H. & Garotta, G. (1990) *Immunological Methods* (Academic, Orlando, FL), Vol. 4, p. 121.
16. Bracher, A., Eisenreich, W., Schramek, N., Ritz, H., Goetze, E., Herrmann, A., Gütlich, M. & Bacher, A. (1998) *J. Biol. Chem.* **273,** 28132–28141.
17. Sambrook, J., Fritsch, E. F. & Maniatis, T (1989) *Molecular Cloning: A Laboratory Manual.* (Cold Spring Harbor Lab. Press, Plainview, NY), 2nd Ed., p. A2.
18. Leslie, A. G. W. (1991) *Crystallographic Computing V,* eds. Moras, D., Podjarny, A. D. & Thierry, J. C. (Oxford Univ. Press, Oxford), pp. 27–38.
19. Collaborative Computational Project, Number 4 (1994) *Acta Crystallogr. D* **50,** 760–763.
20. Huber, R. (1965) *Acta Crystallogr. A* **15,** 23–31.
21. Rossmann, M. G. (1990) *Acta Crystallogr. A* **46,** 73–82.
22. Navaza, J. & Vernoslava, E. (1994) *Acta Crystallogr. A* **51,** 445–449.
23. Turk, D. (1992) Ph.D. thesis (Technical Univ. of Munich, Germany).
24. Jones, T. A., Bergdoll, M. & Kjeldgaard, M. (1990) In: *Crystallography and Modelling Methods in Molecular Design,* eds. Bugg, C. & Ealick, S. (Springer, New York), pp. 189–199.
25. Brünger, A. T. (1992) X-PLOR Version 3.1: A System for Crystallography and NMR (Yale Univ. Press, New Haven, CT).
26. Brünger, A. T., Adams, P. D., Clore, G. M., DeLano, W. L., Gros, P., Grosse-Kunstleve, R. W., Jiang, J.-S., Kuszewski, J., Nigles, M., Pannu, N. S., *et al.* (1998) *Acta Crystallogr. D* **54,** 905–921.
27. Engh, R. A. & Huber, R. (1991) *Acta Crystallogr. A* **47,** 392–400.
28. Kraulis, P. J. (1991) *J. Appl. Crystallogr.* **24,** 946–950.
29. Merritt, E. A. & Murphy, M. E. P. (1994) *Acta Crystallogr. D* **50,** 869–873.
30. Schmid, C. (1992) Ph.D. thesis (Technical Univ. of Munich, Germany).